Journal of Atmospheric and Solar-Terrestrial Physics 73 (2011) 2201–2211

Contents lists available at ScienceDirect

Journal of Atmospheric and Solar-Terrestrial Physics

journal homepage: www.elsevier.com/locate/jastp

Bite-outs and other depletions of mesospheric electrons

Martin Friedrich [a,*], Markus Rapp [b], John M.C. Plane [c], Klaus M. Torkar [d]

[a] Graz University of Technology, Graz, Austria
[b] Leibniz Institute of Atmospheric Physics, Kühlungsborn, Germany
[c] University of Leeds, Leeds, UK
[d] Space Research Institute, Austrian Academy of Sciences, Graz, Austria

ARTICLE INFO

Article history:
Received 22 April 2010
Received in revised form
24 September 2010
Accepted 26 October 2010
Available online 3 November 2010

Keywords:
Noctilucent clouds
Mesosphere
Meteoric dust
Bite-out

ABSTRACT

The ionised mesosphere is less understood than other parts of the ionosphere because of the challenges of making appropriate measurements in this complex region. We use rocket borne *in situ* measurements of absolute electron density by the Faraday rotation technique and accompanying DC-probe measurements to study the effect of particles on the *D*-region charge balance. Several examples of electron bite-outs, their actual depth as well as simultaneous observations of positive ions are presented. For a better understanding of the various dependencies we use the ratio β/α_i (attachment rate over ion–ion recombination coefficient), derived from the electron and ion density profiles by applying a simplified ion-chemical scheme, and correlate this term with solar zenith angle and moon brightness. The probable causes are different for day and night; recent *in situ* measurements support existing hypotheses for daytime cases, but also reveal behaviour at night hitherto not reported in the literature. Within the large range of β/α_i values obtained from the analysis of 28 high latitude night flights one finds that the intensity of scattered sunlight after sunset, and even moonlight, apparently can photodetach electrons from meteoric smoke particles (MSP) and molecular anions. The large range of values itself can best be explained by the variability of the MSPs and by occasionally occurring atomic oxygen impacting on the negative ion chemistry in the night-time mesosphere under disturbed conditions.

1. Introduction

In recent years it has been realised that the composition of the *D*-region plasma is more complicated than previously considered. While it was long thought that the *D*-region was solely composed of electrons and molecular negative ions (the latter primarily during night-time) and positive ions, it is now well established that several aerosol species occur in the relevant altitude range, acquire a charge by processes like electron and ion attachment as well as photoemission and photodetachment, and subsequently contribute to the local charge balance. The two most prominent examples of these aerosol species are mesospheric ice particles and meteoric smoke particles (MSPs). Mesospheric ice particles only occur in the extreme thermal environment of the cold polar summer mesopause region where they lead to phenomena such as noctilucent clouds (NLC) and polar mesosphere summer echoes (PMSE). Owing to the thermal structure, these ice particles exist in narrow layers and hence occasionally lead to spectacular effects on the electron density profile, i.e. electron density depletion which has been termed "electron bite-outs". Meteoric smoke particles on the other hand are thought to occur as a consequence of meteoroid ablation and subsequent formation of secondary metal oxide-containing particles (Saunders and Plane, 2006) with typical radii in the low nanometre size range. Recent rocket (Lynch et al., 2005; Rapp, 2009), radar (Fentzke et al., 2009; Strelnikova et al., 2007), and satellite experiments (Hervig et al., 2009) have confirmed their ubiquitous presence in the entire mesosphere. However, unlike in the case of mesospheric ice particles their quantitative effect on the *D*-region charge balance has hitherto been largely ignored.

In the this paper, we will consider rocket borne *in situ* measurements of absolute electron density using the Faraday rotation technique as well as accompanying DC-probe measurements to study the effect of particles on the *D*-region charge balance. Starting with polar summer conditions, we present several examples of electron bite-outs and discuss their actual depth as well as simultaneous observations of positive ions. Turning then to polar night conditions, we consider whether the available data base of concurrent absolute electron and positive ion density measurements allows us to identify the effect of MSPs.

The number density of free electrons N_e in the ionosphere is the result of a balance between ionisation (rate q) and the effective recombination (rate α_{eff}), neglecting second order effects such as transport and non-steady state. For charge neutrality the number densities of electrons N_e must equal that of (positive) ions N^+, i.e. $N_e = N^+$ if we for the time being neglect negative ions. Since in the mesosphere (the *D*-region) the lifetime of the free electrons is very

* Corresponding author. Tel.: +43 316 873 7449.
E-mail address: martin.friedrich@tugraz.at (M. Friedrich).

1364-6826
doi:10.1016/j.jastp.2010.10.018

short, the following "classical" relation applies:

$$\alpha_{eff} = \frac{q}{N_e^2} \quad (1)$$

The dominating ions in the mesosphere are O_2^+ and NO^+, which have very similar electron recombination rates (Florescu-Mitchell and Mitchell, 2006), but below a distinct boundary located between 70 and 90 km water cluster ions of the type $H^+(H_2O)_n$ and $NO^+(H_2O)_n$ are prevalent (Friedrich and Torkar, 1988). The recombination rates of these cluster ions are about two orders of magnitude larger than those of molecular ions (Florescu-Mitchell and Mitchell, 2006); the nature of the ions is therefore very relevant for the density of free electrons (for a simplified chemical scheme see Fig. 9). Since neither the ionisation rate q, nor the nature of the positive ions changes abruptly with altitude, one can reasonably expect a similarly smooth resulting electron density profile. Fig. 1 shows an example of daytime electron and partial ion densities together with the effective recombination rate obtained by the same rocket flight. Clearly below the transition from molecular to cluster ions the effective recombination rate increases and consequently the plasma density drops significantly.

At times actual N_e profiles show very narrow enhancements located between 90 and 120 km. Usually termed sporadic E layers (E_s), these narrow layers are known to be comprised of metal ions, particularly Fe^+ and Mg^+, because of their very low electron recombination rates above 90 km (Woodcock et al., 2006). Fig. 2 shows a mid-latitude night-time mass spectrometer measurement, which displays two sporadic E layers with enhanced metallic ion concentrations (Roddy et al., 2004).

The otherwise smooth variation of the plasma density with height cannot only have positive excursions as demonstrated above, but at times also deep depletions, often termed bite-outs. Fig. 3 is a collection of high latitude, summer profiles in which all show more or less pronounced bite-outs near the mesopause region. The data for this particular figure are in 1 km steps. Since there is no known ionisation source that could be significantly attenuated over such a small height range, the alternative is that there is a limited height region where free electrons "somehow" disappear. Since all the cases shown in that figure are from the high latitude summer, we are dealing with daytime conditions (solar zenith angles between 47.5 and 93.2°). Empirically the day/night transition occurs when the region under investigation is illuminated from below when a ray from the Sun grazes the ozone layer (assumed at 30 km). For the mesosphere this corresponds to a solar zenith angle of 98°, a value which is based both on theoretical arguments (Turco and Sechrist, 1972), but was also found in the analysis of ionospheric absorption data (Stauning, 1996). This is primarily caused by the disappearance of photodetachment by visible light, which at night leads to negative ions and in consequence to a loss of free electrons.

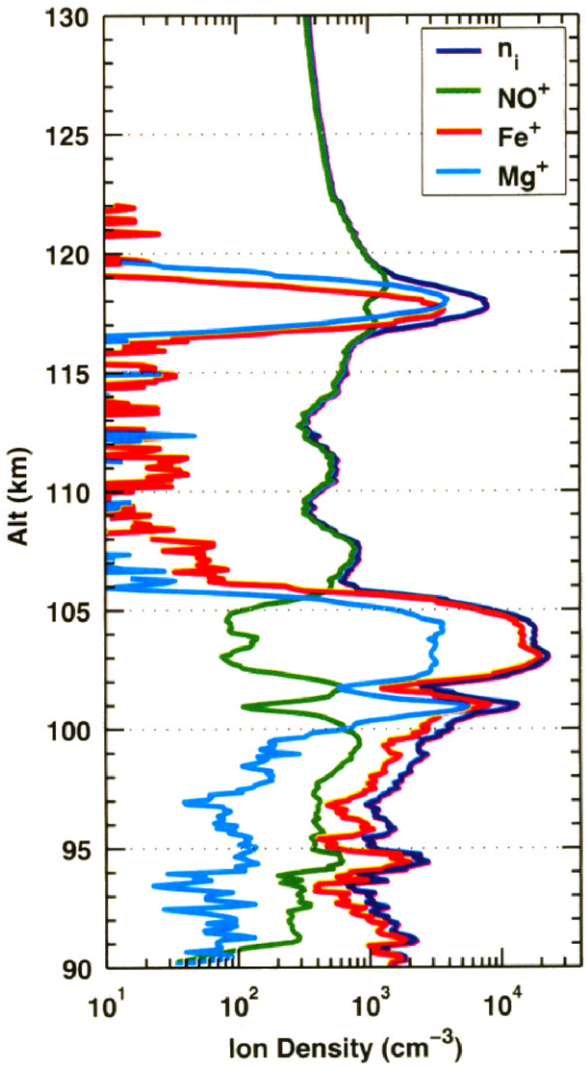

Fig. 2. Partial ion densities measured in a night-time, mid-latitude rocket flight (Roddy et al., 2004). The prominent layer at 118 km coincides with metal ion densities exceeding the otherwise dominating NO^+, whereas in the layers between 100 and 105 km the metal ions anti-correlate with NO^+.

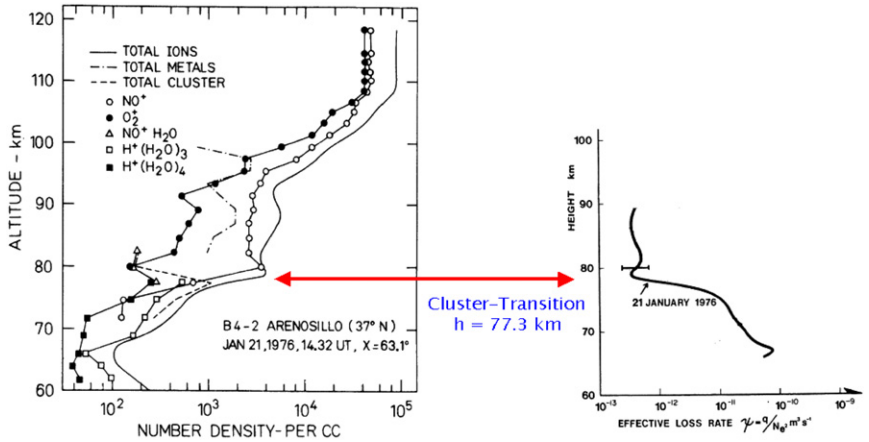

Fig. 1. Partial ion densities measured during daytime at mid-latitudes (left panel; Arnold and Krankowsky, 1979) and the effective recombination rate derived from the same rocket flight (right panel; Thrane et al., 1979). Note the distinct increase of the recombination rate below 77.3 km where cluster ions dominate.

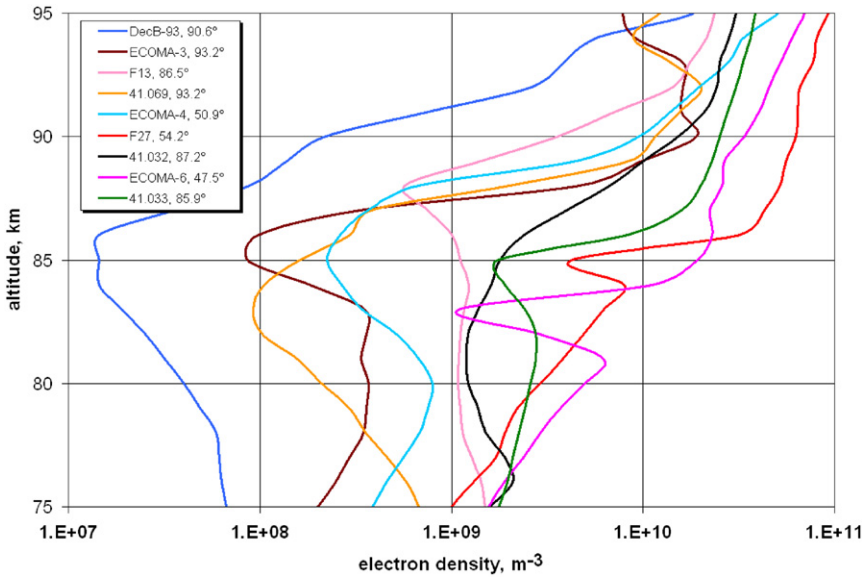

Fig. 3. Summer electron density profiles (at solar zenith angles ranging from 47.5 to 93.2°) from high latitudes showing bite-outs. The values shown are based on radio wave propagation results only. Of the nine rockets at least seven were intentionally launched in conditions where bite-outs can be expected (NLC, PMSE, see text).

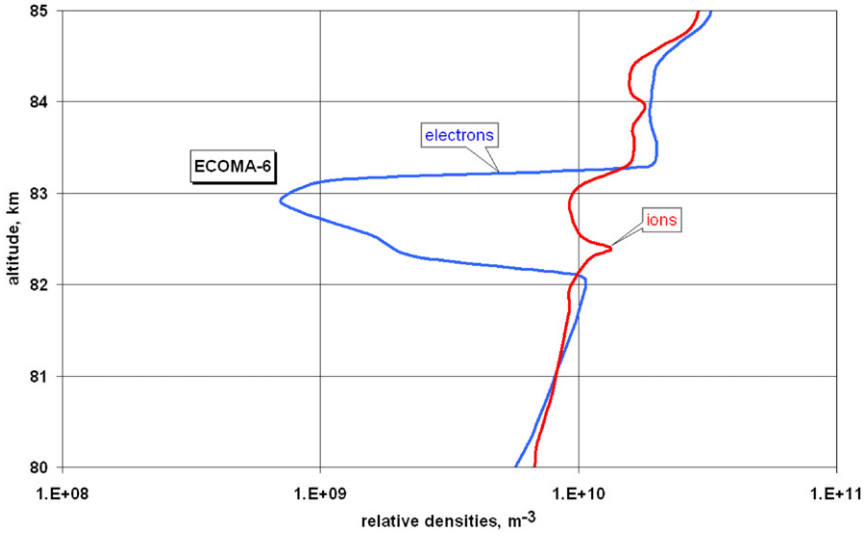

Fig. 4. Blow-up of the electron bite-out measured by a DC probe aboard rocket ECOMA-6. Note that only the electrons, but not the ions are depleted. Given the solar zenith angle of 47.5° the difference between the density of positive ions and electron cannot be due to negative ions.

Apart from the obvious lack of ionising radiation from the Sun, as an indirect consequence thereof the night-time *D*-region is characterised by more water cluster ions leading to a larger effective recombination rate, and by the possibility that negative ions can exist. Hence charge neutrality $N^+ = N_e + N^-$ applies with N^- being the number density of negative ions. Above about 83 km there is little difference between day and night as far as the ion chemistry is concerned. One should therefore expect that the bite-outs in electron density should also exist in the density of positive ions. However, the blow-up of the deep bite-out observed in flight ECOMA-6 shows that only the electrons – in contrast to the (positive) ions – are depleted (Fig. 4).

2. Data

In the above discussion we have taken the plasma densities depicted in Figs. 1–4 at face value; however, a critical assessment of the reliability of these data is expedient before embarking on further analysis and a search for explanations. All data used here are based on sounding rockets, not least because ground-based electron density measurements cannot resolve bite-outs on the order of a kilometre or less (e.g. Fig. 4). Rocket borne probes potentially have a high temporal resolution, which is largely only limited by the available telemetry sampling rate; however, because of aerodynamic considerations often only the largest value per rocket spin period is considered to represent the true plasma density. The simplest electron probe consists of a positively biased sensor that collects electrons from "nearby". The actual current depends on the bias itself relative to the plasma potential, which therefore makes such an instrument sensitive to changes of the rocket potential (Smith, 1969). Since the electron current collected by the probe must be compensated by a corresponding return current provided by much less mobile ions, the area ratio between probe and payload body must be very small; Szuszczewicz (1972) recommends 10^{-4} to assure that the payload potential remains

essentially unaffected by the electron current drawn by the probe. Positive ions, on the other hand, are collected by gridded spheres at payload potential (which is close to that of the plasma) with a negatively biased inner collector. The current measured by such an arrangement is almost exclusively determined by the probe's cross section and the rocket velocity, which control the number of ions entering the shielded volume, but not by the actual bias of the inner collector (Sagalyn et al., 1963; Folkestad, 1970). Due to the much larger inertia of the ions, the payload potential has only a small effect on the collected current compared to the electron current, and the return current can easily be provided by the mobile electrons and thus the payload potential is virtually unaffected by the ion probe itself. The plasma densities depicted in Fig. 4 are the nominal (uncalibrated) values from such an arrangement of probes (Fig. 5). Conceivably the deep bite-out of the electron density could be due to a drastic change of the payload potential (i.e. going negative); despite the only marginal sensitivity of the ion probe to payload potential changes one would still expect some anti-correlation of the two probe currents, which – at least in this example – is not evident.

In situ measurements with probes potentially have a good height resolution, but are all uncertain in their absolute values, notably in the relatively dense neutral background of the mesosphere. A reliable method to obtain electron densities in the *D*- to *E*-region makes use of the dual and complex properties of the ionosphere's refractive index for HF radio waves. The instrumentally simplest radio wave propagation experiment of this kind, i.e. measuring the Faraday rotation of a wave transmitted from the ground, uses the rocket spin itself to determine the orientation of the wave polarisation. Consequently the resolution is tied to the rocket spin of between 3 and 5 rps, which results in a typical height resolution usually not better than about 1 km. The raw data (integral Faraday rotation) is proportional to the electron content between ground and payload and one has to assume stability of the ionosphere for the duration of the measurement (typically 2 min of the rocket's upleg). Fortunately up to the *E*-layer the electron densities steadily increase and a possible change of the underneath ionosphere is not too critical. Despite these limitations the attraction of the method is that it is completely immune to payload charging, plasma sheath formation or aerodynamic effects. There is ample literature describing the method (e.g. Mechtly et al., 1967), the detection limits and the optimal choice of the sounding frequencies was addressed by Jacobsen and Friedrich (1979) and an assessment of this, relative to other methods is, e.g., given by Thrane (1974).

Based both on theoretical arguments and empirical confirmatons (Friedrich and Torkar, 1995), negative ions cannot exist in a low neutral density background and in the presence of appreciable concentrations of atomic oxygen; hence, above 90 km under all circumstances the number density of electrons N_e must equal that of the positive ions N^+. An ion density profile calculated using the rocket velocity, the probe's cross section, grid transparency, etc. can thus be normalised to the electron density profile above 90 km. One generally assumes the normalisation factor to be height independent. Based on many rocket flights where both the relative ion densities and absolute electron densities from a wave propagation experiment were available over a larger height region this was found to be an acceptable assumption. Fig. 6 shows electron and (normalised) ion densities of one of the high latitude summer flights of Fig. 3. The solar zenith angle in this particular case was 90.6°, i.e. daytime as far as ion (recombination) chemistry is concerned. The bite-out extends over almost 20 km, hence the height resolution of the wave propagation electron densities is good enough to unambiguously identify the depth of the depletion. *Assuming* constancy of the normalisation factor of the ion probe over almost 30 km, near 70 km electrons and ions seem to converge, which supports the assertion of a constant normalisation factor for the probe. The peak in the ion density at 83 km coincided with a layer of ice particles (NLC, see below). An ion density enhancement coincident with a bite-out was, e.g., also observed by Havnes and Næsheim (2007) under similar conditions. The model calculations carried out by Lübken and Rapp (2001) for this particular case suggest that this is to be expected for very deep bite-outs. The line marked electrons shows data of a capacitance probe, which only properly functions at low collision frequencies (low pressure), i.e. in the present case above 91 km; the values below that height (dotted line) are therefore not related to electron densities.

3. Daytime situation

Clouds near 83 km were first reported independently by several authors in 1885 (Backhouse, 1885; Jesse, 1885; Leslie, 1885) and

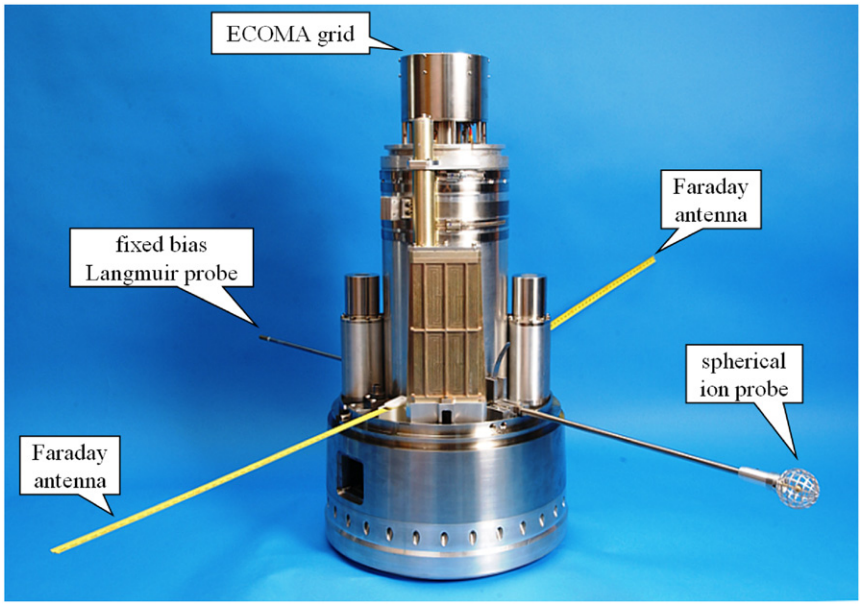

Fig. 5. Arrangement of plasma diagnostic instruments on the top section of a sounding rocket (ECOMA series).

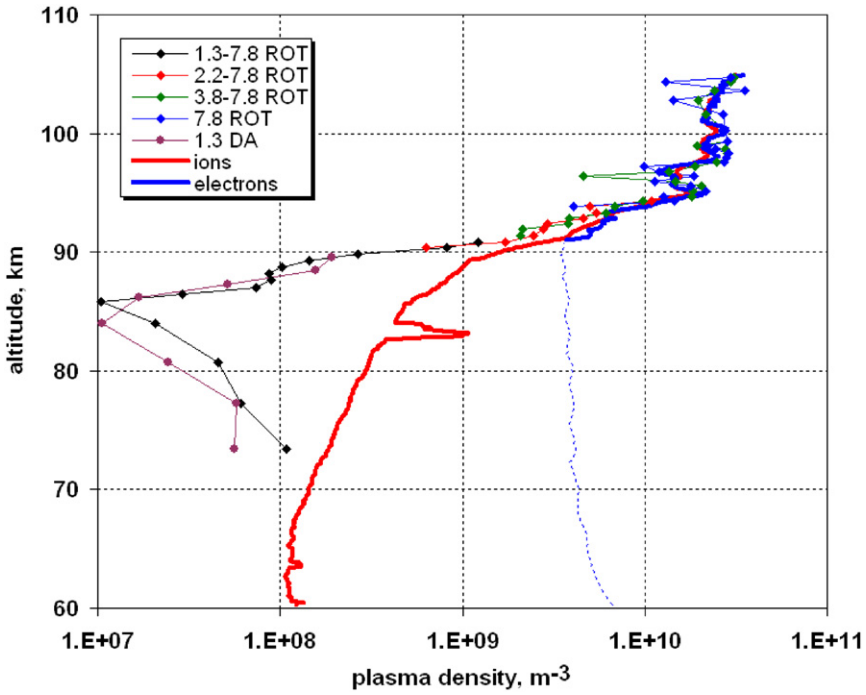

Fig. 6. Plasma densities measured by a twilight flight in the polar summer (ESRANGE, Sweden, August 2, 1993, solar zenith angle 90.6°). The symbols are due to data from various sounding frequencies. The curve labelled electrons is due to a capacitance probe, which only yields usable data when the collision frequency is low (in this case above 91 km). This curve and the one for ions are normalised to the wave propagation data above 93 km.

were initially attributed to the Krakatau eruption two years earlier. These so-called noctilucent clouds (NLC) only occur near the extremely cold summer mesopause and poleward of about 52°. Based on various optical methods the nature of the particles were determined to be water ice (Hervig et al., 2001) with diameters ranging from 10 to 100 nm (Thomas and McKay, 1985). Attachment of free electrons onto these relative large ice particles is generally considered to be the main process removing free electrons in rather thin layers. The raw data of the wave propagation experiments as described above are incremental Faraday rotation of the signal transmitted from the ground (deg/km). The electron densities in the deep bite-outs is so low that the raw data simply show no detectable incremental rotation of the wave polarisation orientation. Thus for the depth of these very narrow bite-outs we have to rely on normalised probe measurements, but the height where they occur can usually be obtained from the radio wave experiments (e.g. Croskey et al., 2004). A recent measurement (rocket 41.033) demonstrating the relation between ice particles and bite-outs is given in Fig. 7. The depth of the electron density depletion is measured by the electrostatic probe, but the wave propagation data confirms the altitudes of the bite-outs and provides the normalisation to absolute values above and below the bite-out (see also the relevant curve in Fig. 3). The data from the blunt probes (impact detectors) indicate a clear net dominance of negatively charged heavy particles, which supports the assertion that electrons are scavenged by their attachment to ice particles.

Another test of the hypothesis that mesospheric ice causes the depletion of electron densities is given in Fig. 8. This flight (ECOMA-6) carried upward-looking photometers measuring sunlight at 224 nm scattered by the overhead ice cloud. From the analysis of the scattering angle typical diameters of 50 nm were found in this particular flight, whereas simply measuring the intensity as a function of altitude (left panel) yields information on the location, and the density of the NLC layer (central panel). This differentiated overhead intensity exactly peaks at the height where the electrons are depleted (right panel).

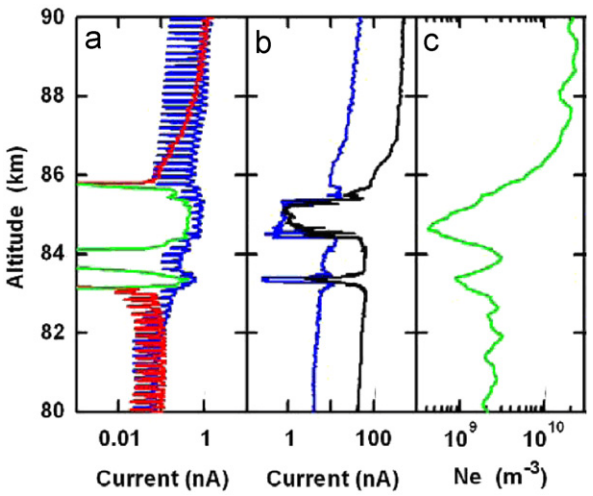

Fig. 7. Electron density bite-out and associated parameters (rocket 41.033; after Croskey et al. (2004). Panel (c) is the electron density obtained from the wave propagation experiment (upleg), whereas the current shown in panel (b) (black line) represents the electron density from an onboard probe on upleg. The green line in panel (a) is the net negative current observed by Faraday cup particle detectors.

4. Night-time

Identifying a bite-out for daytime conditions is relatively straightforward: either simply finding extreme depletions (*cf.* rocket flights ECOMA-6, F27, or 41.033 in Fig. 3), or by comparing electron and ion densities (Figs. 4 and 6). The latter criterion is a very strong argument for a daytime bite-out because negative ions cannot exist where these inequalities between the number densities of positive ions and electrons are observed.

At night the simple Eq. (1) has to be extended to account for negative ions N^-.

$$\alpha_{eff} = (1+\lambda)(\alpha_D + \lambda\alpha_i) = \frac{q}{N_e^2} \tag{2}$$

where $\lambda = N^-/N_e$, α_D is the dissociative recombination (electron-positive ion) coefficient and α_i the ion–ion recombination coefficient.

Fig. 9 shows an ion-chemistry scheme adequate for a qualitative understanding of the behaviour to be described below. In the present context we need to look at the chemistry of the negative species that are here reduced to only electrons and X^- representing all negatively charged species. The negative ions X^- are formed by attachment of electrons to O_2, which requires the presence of a third body, here indicated by M (i.e., N_2+O_2). The reverse reaction is *via* atomic oxygen and by photodetachment hν. This simple scenario explains why negative ions drastically disappear at higher altitudes (too little O_2 and M, and too much O) and as soon as sunlight is visible (solar zenith angle $< 98°$; *cf.* Stauning, 1996). For conditions of steady-state – which we always tacitly assume – the formation of negative ions by three-body collision is principally balanced by three loss processes on the right-hand side of the equation.

$$N_e\beta M^2 = N^-(\gamma + \alpha_i N^+ + k[O]) \tag{3}$$

where β is the attachment rate (note that $O_2 \sim 0.2M$, hence the term M^2 in Eq. (3)), M the neutral number density, k the electron detachment by atomic oxygen and γ the photodetachment rate.

For night-time conditions, i.e. for which we have data on electron *and* ion densities from many flights, we may largely neglect reactions involving [O] and ignore γ, so that Eq. (2) reduces to

$$N_e\beta M^2 = N^-\alpha_i N^+ \tag{4}$$

for charge neutrality (i.e. $N_e + N^- = N^+$) one can thus can rearrange Eq. (4) as

$$N_e = \frac{N^+}{1+(\beta/\alpha_i)(M^2/N^+)} \tag{5}$$

The above relation shows that with increase in altitude (decrease in neutral number density M) N_e rapidly approaches N^+, i.e. negative ions do not exist at significant concentrations. In other words, given known (and height-independent) rates for attachment and ion–ion recombination, one can derive the density of electrons from that of positive ions, or *vice versa*. Rocket F69 was launched from Andøya Rocket Range in February 1984 under full night conditions (solar zenith angle 116.4°). The payload carried both a wave propagation experiment to establish absolute electron densities and a probe to measure positive ions (Fig. 10, left panel). The ion probe data were normalised to the electron density values above 90 km, below that height the difference between electrons and positive ions is – according to conventional concepts – due to negative ions. The dashed line is obtained from the density of positive ions using Eq. (5). A value of $\beta/\alpha_i = 5\times10^{-26}$ cm^3 was found to provide the displayed agreement between measured and inferred electron density. This value is somewhat lower than one would expect using laboratory values for β (10^{-31} cm^6 s^{-1}; Phelps,

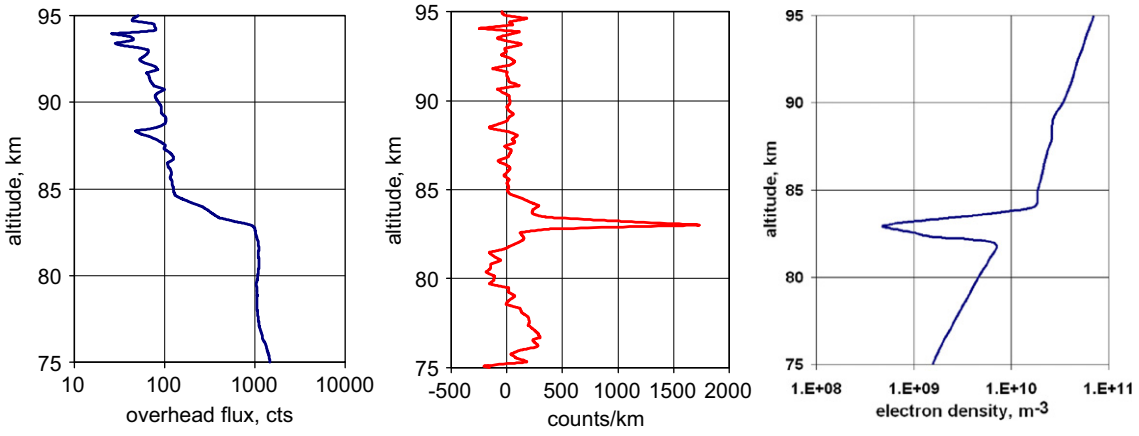

Fig. 8. Scattered light intensity at 224 nm (in arbitrary units) looking upward (left panel), its derivative (central panel), which is a measure of the density of the scattering particles, and the electron density (calibrated probe data, right panel). Flight ECOMA-6; photometer data courtesy Misha Khaplanov.

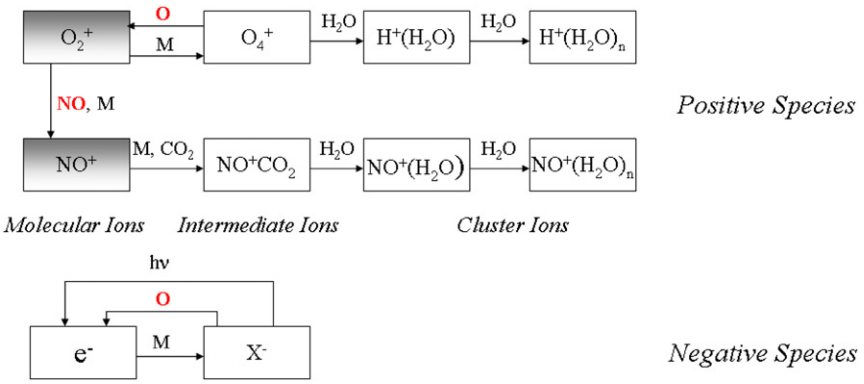

Fig. 9. Simplified ion-chemistry of the *D*-region. Ions in the shaded boxes are the ones primarily produced. For graphical reasons the reactions between the negative species (e^- and X^-) to all of the positive species are omitted. O = atomic oxygen, M = background mass density and NO = nitric oxide.

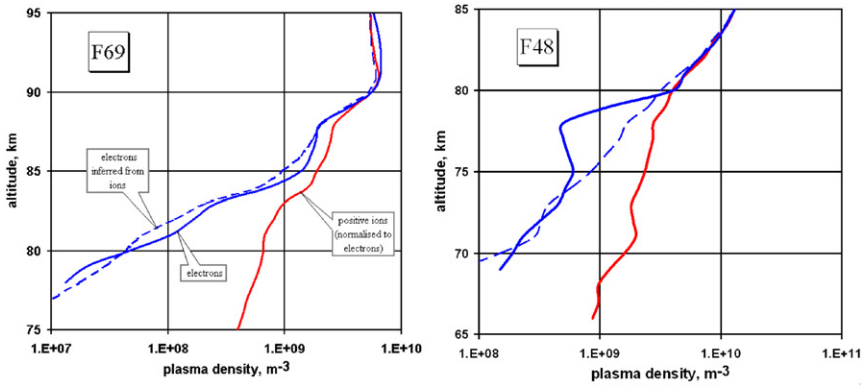

Fig. 10. Electron and ion densities measured by the rocket flight F69 under full darkness and outside the NLC season (left panel, February 1984). The dashed lines (inferred electrons) are obtained using Eq. (4). The right panel under similar conditions (except for larger riometer absorption; note the different scales!) is a case where the same relation does not everywhere produce such good agreement between measured and inferred electron density.

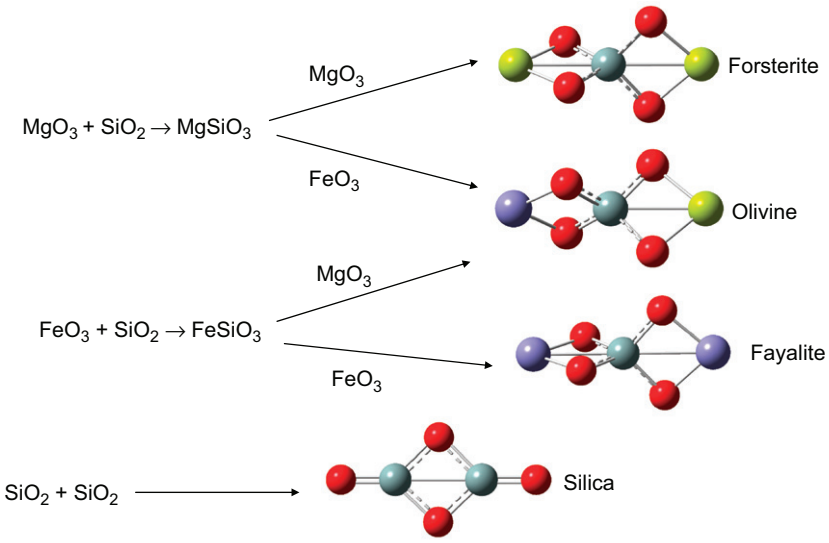

Fig. 11. Structures of possible 0.5 nm radius meteoric smoke particles formed from mixtures of Mg–Fe–Si–O4 (blue = Fe; yellow = Mg; grey = Si; red = O). Calculations at the B3LYP/6-311+g(2d,p) level of quantum theory.

1969) and α_i (4×10^{-7} cm^3 s^{-1}; Peterson et al., 1971), but probably still within the uncertainties of these early laboratory results.

The corresponding exercise with the rocket F48 shows a different behaviour: obviously no single β/α_i can be used for the entire altitude region for agreement between measured and inferred electron density, but rather a much smaller α_i (or larger β) seems to apply around 77 km. This is surprising because the ion–ion recombination rate coefficient α_i is governed by the long-range Coulombic attractive forces between the oppositely-charged ions (Smith, 1980), and so does not vary much for recombination of NO^+ and O_2^+ with small anions. β describes the attachment of an electron to O_2. Also, both rate coefficients have very small temperature dependences (Smith, 1980). Analogous to the daytime (summer) situation we therefore speculate that some other scavenger removes free electrons beyond what one would expect from attachment to neutral atmospheric molecules. The most likely candidate is MSPs.

Laboratory experiments (Saunders and Plane, 2006) have shown that iron and magnesium oxides recombine readily with silica (SiO_2) to form olivines $Mg_xFe_{2-x}SiO_4$, ranging from Forsterite ($x=2$) to Fayalite ($x=0$), and that SiO_2 also polymerises with itself (Fig. 11). These molecules, which are about 0.5 nm in radius, are examples of the smallest MSPs, which will form from the recondensation of meteoric vapours. Electronic structure calculations (at the B3LYP/6-311+g(2d,p) level of theory) show that the electron affinities for these molecules are large, ranging from 1.9 to 2.4 eV. Because the molecules are polyatomic and bind electrons strongly, the rate coefficients for electron attachment at mesospheric pressures are likely to be large $\sim2\times10^{-7}$ cm^3 s^{-1} (Troe et al., 2007). In contrast, the electron affinity of O_2 is only 0.43 eV, and so the corresponding rate coefficient for electron attachment is very small: $\beta M=3\times10^{-17}$ cm^3 s^{-1} around 85 km. Thus, even though the MSP concentration is only a few thousand cm^{-3} (Strelnikova et al., 2009), the rate of electron removal is comparable to attachment to O_2. Furthermore, the electrons are strongly enough attached that atomic O is not able to destroy the MSP anions, in contrast to O_2^-. Nevertheless, photodetachment is still likely in the daytime, and could in principle be achieved by photons at wavelengths shorter than 600 nm (i.e. most of the visible spectrum). Hence, MSPs should cause significant removal of electrons at night, but the depletion during daytime would be limited.

Indeed, the existence of negatively charged (meteoric) smoke particles has been measured *in situ* between 70 and 90 km outside the polar regions (Gelinas et al., 1998) and outside the NLC season (Rapp et al., 2010), i.e. over an altitude range much larger than the

NLC region that causes the more pronounced daytime bite-outs in the polar summer. Using a novel algorithm described by Strelnikova et al. (2007), negatively charged particles have also been inferred from the echoes of the Arecibo radar between 85 and 92 km (Fentzke et al., 2009).

The attachment of electrons to MSPs can be treated with analogous expressions to Eqs. (3)–(5), i.e.

$$N_e\beta_d N_d^0 = N_d^-(\gamma_d + \alpha_d^i N^+) \tag{6}$$

β_d is the attachment rate of electrons to neutral MSP, N_d^0 the number density of neutral MSP, N_d^- the number density of negatively charged MSP, γ_d the photodetachment rate and α_d the attachment rate of positive ion to negatively charged MSP.

As before, for night-time conditions, we may neglect photodetachment processes, so that Eq. (6) reduces to

$$N_e\beta_d N_d^0 = N_d^-\alpha_d^i N^+ \tag{7}$$

For charge neutrality (i.e. $N_e + N_d^- = N^+$) one can formally rearrange Eq. (7) to a similar form as Eq. (5), i.e.

$$N_e = \frac{N^+}{1+\frac{\beta_d N_d^0}{\alpha_d^i M^2}\frac{M^2}{N^+}} = \frac{N}{1+\frac{\beta^*}{\alpha^*}\frac{M^2}{N^+}} \tag{8}$$

Note, that Eq. (8) contains N_d^0 and hence an additional quantity, which cannot be eliminated. However, since no experimental information on N_d^0 is available, we consider it as a valid initial step to treat β/α_i in Eq. (5) as being due to scavenging both by molecules and MSPs (and being well aware that β^*/α^* in Eq. (8) also depends on the neutral number density and the concentration of neutral MSPs). If β/α_i in Eq. (5) is then adjusted at every kilometre for perfect agreement between measured and inferred electron density, one obtains values covering almost five orders magnitude. Let us test whether any systematic behaviour can be found in this seemingly chaotic result. Electron scavenging, expressed by the factor β/α_i, might be expected to depend on the following factors:

(1) season: according to theoretical models (Bardeen et al., 2008; Megner et al., 2008) there should be more MSPs in winter than in summer because of the convergence of the meridional circulation over the winter pole,
(2) temperature: the chemical reactions are temperature dependent,
(3) solar zenith angle: even after sundown the sunlight scattered by the geocorona varies with solar zenith angle,
(4) moonlight: although only a fraction of direct sunlight, it may still suffice to photodetach and
(5) altitude: according to atmospheric models of MSP formation (Bardeen et al., 2008; Megner et al., 2008), growth of MSPs by coagulation will lead to larger particles, but a consequent decrease of the number of particles below 80 km.

Our β/α_i data originate from 28 rocket flights which all happened to be performed in the auroral zone (67° to 69°N) and – because of the requirement of full darkness – are therefore all from the winter season (October 28 to April 9). Atmospheric circulation models of MSPs (Bardeen et al., 2008; Megner et al., 2008) predict a fairly constant density of MSPs (within a factor of 1.5) during this time period in the Arctic mesosphere, so seasonality is unlikely to be a major factor in the variability in the data. This still leaves 4 parameters, which attachment could depend on. For the test of a dependence on temperature the MSIS model values are used, unless temperatures were actually measured by the same rocket or in the same salvo. In contrast to summer conditions where MSIS does not provide an adequate description of mesospheric temperatures (Friedrich et al., 2004), we are dealing with winter observations where both MSIS and CIRA largely agree with local measurements (Lübken and von Zahn, 1991). A 4-dimensional correlation analysis of β/α_i shows no significant temperature dependence, which would be expected because the temperature dependences of electron attachment and ion–ion recombination reactions are small (Smith, 1980).

This now leaves us with the task of fitting the data to a 3-dimensional function, i.e. of solar zenith angle, moonlight and altitude, whereof the correlation with altitude turns out to be inconclusive. This might be expected since at lower altitude the MSPs become larger through coagulation, but on the other hand there are as a result fewer of them. We now try to separate the impact of moonlight from that of scattered sunlight. Many of the 28 rocket payloads carried optical instruments and were therefore intentionally launched in complete absence of moonlight. The variation of β/α_i of these 15 rockets as a function solar zenith angle is shown in Fig. 12. There is a trend to larger values later in the night, i.e. – assuming that the ion–ion recombination is unaffected – more electron attachment, or less photodetachment, seems to be occurring. The solar emissions that are scattered in the geocorona are primarily Lyman-α, and to lesser extent, Lyman-β. According to

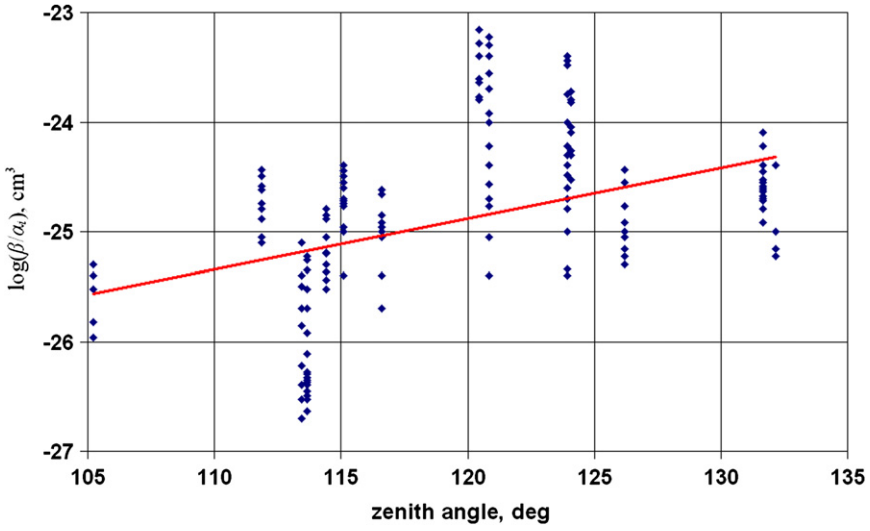

Fig. 12. Dependence of β/α_i on solar zenith angle. The points were taken in absence of any moonlight and are from all altitudes in the dataset (60 to 92 km); normalised to a solar zenith angle of 120° according to the dependence in the previous figure. The red line is an RMS fit. (For interpretation of the references to color in this figure legend, the reader is referred to the web version of this article.)

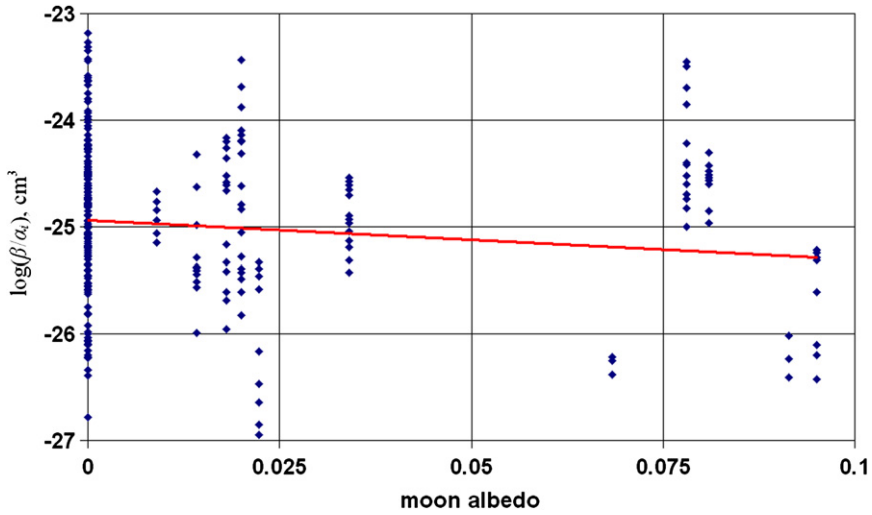

Fig. 13. Dependence of β/α_i on moonlight relative to sunlight in the visible (555 nm). The points are from all altitudes in the dataset (60 to 92 km), normalised to a solar zenith angle of 120° according to the dependence in the previous figure. The red line is an RMS fit. The data on the left of the diagram (moon albedo = 0) are the ones used in the previous figure. (For interpretation of the references to color in this figure legend, the reader is referred to the web version of this article.)

theoretical calculations (Strobel et al., 1974, 1980) one can expect a reduction of the fluxes of these solar lines by about a factor of three in the zenith angle range covered in the figure. A connection with ionisation due to these fluxes appears unlikely in view of the fact that no such relation could be found with riometer absorption (between 0 and 2.9 dB), a proxy for a much larger variation of ionisation rates.

The Moon acts as a reflector of sunlight with a maximum albedo of 0.135 in the visible (at 555 nm; Kieffer and Stone, 2005) and of 0.04 for much of the UV (125 to 184 nm; Henry et al., 1995). The threshold wavelengths relevant for the detachment of electrons from the most common negative ions are 317.9 nm (NO_3^-; Smith et al., 1979), 427.6 nm (CO_3^-; Cosby et al., 1976) and 2883.6 nm (O_2^-; Cosby et al., 1976). The estimated wavelength threshold to detach electrons from MSPs is about 600 nm, according to our quantum calculations described above. Hence, moonlight in the visible range should be able to free attached electrons both from molecules *and* from MSPs. In order to separate the impact of scattered light from moonlight, we normalise the data to the mean solar zenith angle of 120° by applying the dependence shown in Fig. 12 (red line). Fig. 13 depicts the relation β/α_i as a function of Moon albedo in the visible using the relation between moon phase angle and reflectance according to Kieffer and Stone (2005). Again there is a negative correlation between β/α_i and moonlight (or, presumably, a positive correlation between moonlight and photodetachment). Interestingly for full darkness (low moon albedo, large zenith angle) β/a_i comes close to what one expects from the laboratory values (*cf.* Section 4).

Photodetachment competes with ion–ion recombination to remove negative ions. The ion–ion removal rate is around 4×10^{-4} s^{-1}, since α_i is 4×10^{-7} cm^3 s^{-1} and N^+ is typically 10^3 cm^{-3} between 70 and 85 km (Fig. 10). If the increase by about one order of magnitude of β/α_i in Fig. 12 when the solar zenith angle changes from 105° to 132° is caused by a decrease in the photodetachment rate, then the photodetachment rate due to geocoronal light scattering shortly after the solar terminator moves above the mesosphere is $\sim 4 \times 10^{-3}$ s^{-1}.

The huge scatter is larger than can realistically be ascribed to the different instrumental configurations. We therefore surmise that this arises from several factors: the variability of the meteoric flux reaching the mesosphere, and hence the concentration of neutral MSPs; transport of the metallic vapours to altitudes below 90 km where MSPs form; and transport of atomic O from above 90 km, which affects the formation of negative molecular ions. Transport by tides, dissipating gravity waves and turbulence from breaking waves can all cause substantial short-term variability (on a time scale of hours) in the MSP and atomic O concentration in the region below 90 km where electron depletion becomes significant (Fig. 10). Note that further down in the atmosphere below about 80 km, atomic O effectively disappears at sunset (through recombination with O_2). In addition, the number density of MSPs is expected to decrease with decreasing altitude while at the same time the neutral air density increases exponentially. Assuming reasonable numbers for the MSP number density and the electron MSP-attachment rate (e.g. Rapp, 2000), one can estimate that the electron loss rates due to attachment to MSPs and neutrals attain approximately equal values at about 80 km. Hence, below that altitude, the formation of negative ions rather than the attachment to MSPs will generally be the dominant depletion process.

5. Conclusions

Electron densities in the mesosphere can have excursions to larger values, which are basically understood as being due to metallic ions, but can also exhibit pronounced depletions. Careful analysis of data obtained from suitably instrumented sounding rockets has confirmed that these small-scale and deep depletions are real and not instrumental effects. In the summer polar ionosphere they are caused by the ice particles, which comprise NLCs, onto which free electrons attach. But also outside the NLC season and altitude region electrons are scavenged, although the depletions are – at first sight – not as striking. The most likely process for these depletions is attachment onto meteoric smoke particles, which can occur at all latitudes and seasons; this process we assume to be active in parallel to, and competing with the usual chemistry of negative ions. Irrespective of the actually dominating process, the electron loss appears to depend on both the intensity of scattered sunlight as well as on moonlight. The high variability of this additional electron loss may be explained by a corresponding variability of the MSP. In addition, under disturbed conditions atomic oxygen can at times – even at night – be found at altitudes below the usual ledge near 85 km (Dickinson et al., 1987); in such cases "conventional" electron scavenging by attachment to molecules will be impeded and appear as reduced attachment. At this stage the very limited amount of data from only 28 suitably instrumented rocket flights only allows to draw qualitative conclusions, but does not permit to arrive at quantitative results.

Table 1
Rocket flights used for the β/α_i analysis in chronological order (SZA=solar zenith angle).

code	Year	Month	Day	Time UT	Range	SZA deg	Riometer dB @ 27.6 MHz	Moon albedo	From km	To km	Temperature
F20	1968	4	9	20:38	Andøya	99.2	2.87	0.034	65	80	MSIS
SA1/1	1968	10	24	21:56	ESRANGE	123.9	0.59	0.000	67	82	MSIS
SA1/3	1969	1	18	19:23	Andøya	120.9	0.90	0.000	68	84	MSIS
F21	1969	11	26	00:36	Andøya	128.5	0.59	0.064	72	77	MSIS
F22	1970	3	23	22:58	Andøya	109.6	0.10	0.095	70	83	MSIS
F31	1972	2	13	23:20	Andøya	124.1	0.35	0.000	77	85	MSIS
F32	1973	1	27	18:32	Andøya	114.4	0.44	0.000	71	84	MSIS
S18-2	1976	2	21	19:42	ESRANGE	115.1	2.59	0.000	60	74	MSIS
S18-1	1977	1	15	00:05	ESRANGE	131.7	0.96	0.000	69	86	MSIS
F48	1978	3	1	01:13	Andøya	115.3	0.28	0.020	69	85	MSIS
F47	1978	3	1	01:13	Andøya	115.3	0.28	0.020	72	82	MSIS
33.017	1980	10	18	02:08	Andøya	111.9	0.92	0.000	66	76	MSIS
F54	1980	11	11	01:12	Andøya	126.2	0.17	0.000	76	85	MSIS
F53	1980	11	16	03:31	Andøya	113.7	1.76	0.000	66	76	MSIS
F55	1980	11	16	03:31	Andøya	113.7	1.76	0.000	70	76	MSIS
F56	1980	11	28	03:25	Andøya	116.8	1.32	0.018	70	75	MSIS
F52	1980	11	28	03:25	Andøya	116.8	1.32	0.018	69	77	MSIS
F66	1984	1	6	21:55	Andøya	132.2	0.14	0.000	77	86	measured
F68	1984	1	13	20:00	Andøya	124.8	0.29	0.022	70	84	MSIS
F67	1984	1	25	16:39	Andøya	105.2	0.05	0.000	79	83	measured
F70	1984	1	31	18:31	Andøya	113.5	0.28	0.000	71	81	MSIS
F69	1984	2	10	02:40	Andøya	116.4	0.02	0.009	78	83	MSIS
F64	1984	2	16	01:20	Andøya	119.8	0.86	0.078	74	90	measured
F65	1984	2	18	00:22	Andøya	121.6	0.28	0.081	70	82	measured
F75	1987	10	21	21:33	Andøya	120.5	0.55	0.000	66	72	MSIS
F74	1987	11	12	21:33	Andøya	125.9	0.45	0.014	71	86	MSIS
Rexus	2004	10	28	19:49	ESRANGE	120.1	0.02	0.091	85	89	MSIS
HotPay-2	2008	1	31	19:14	Andøya	116.6	0.04	0.000	84	92	MSIS

Table 2
Other rocket flights referred to in the paper.

Code	Year	Month	Day	Time UT	Range	SZA deg	Riometer dB@27.6 MHz	Data shown in Fig.
F13	1966	6	26	21:47	Andøya	86.5	0.64	3
F27	1971	8	8	12:12	Andøya	54.2	0.60	3
F43	1976	1	21	14:32	El Arenosillo	63.1	NA	1
DecB-93	1993	8	2	01:02	ESRANGE	90.6	0.03	3
41.032	2002	7	1	23:56	Andøya	87.2	0.25	3
41.033	2002	7	5	00:47	Andøya	85.9	0.54	3
27.144	2003	7	1	07:50	Wallops	108.5	NA	2
41.069	2007	8	3	22:51	Andøya	93.2	0.02	3
ECOMA-3	2007	8	3	23:22	Andøya	93.2	0.02	3
ECOMA-4	2008	6	30	13:22	Andøya	50.9	0.00	3
ECOMA-6	2008	7	12	10:46	Andøya	47.5	0.97	4

Acknowledgements

The data used in this report were predominantly obtained from measurements in various projects funded by the Austrian Research Fund (FWF).

Appendix

See Tables 1 and 2

References

Arnold, F., Krankowsky, D., 1979. Mid-latitude lower ionosphere structure and composition measurements during winter. J. Atmos. Terr. Phys. 41, 1127–1140.
Backhouse, T.W., 1885. The luminous cirrus clouds of june and july. Met. Mag. 20, 133.
Bardeen, C.G., Toon, O.B., Jensen, E.J., Marsh, D.R., Harvey, V.L., 2008. Numerical simulations of the three-dimensional distribution of meteoric dust in the mesosphere and upper stratosphere. J. Geophys. Res. 113, D17202. doi:10.1029/2007JD009515.
Cosby, P.C., Ling, J.H., Peterson, J.R., Moseley, J.T., 1976. Photodissociation and photodetachment of molecular negative ions. III—ions formed in $CO_2/O_2/H_2O$ mixtures. J. Chem. Phys. 65, 5267–5274.
Croskey, C.L., Mitchell, J.D., Goldberg, R.A., Blix, T.A., Rapp, M., Latteck, R., Friedrich, M., Smiley, B., 2004. Coordinated investigation of plasma and neutral density fluctuations and particles during the MaCWAVE/MIDAS summer 2002 program. Geophys. Res. Lett. 31, 24. doi:10.1029/2004GL020169.
Dickinson, P.H.G., Witt, G., Zuber, A., Murtagh, D., Grossmann, K.U., Brückelmann, H.G., Schwabbauer, P., Baker, K.D., Ulwick, J.C., Thomas, R.J., 1987. Measurements of odd oxygen in the polar region on 10 February 1984 during MAP/WINE. J. Atmos. Terr. Phys. 49 (7/8), 843–854.
Fentzke, J.T., Janches, D., Strelnikova, Irina, Rapp, M., 2009. Meteoric smoke particle properties derived using dual-beam arecibo UHF observations of *D*-region spectra during different seasons. J. Atmos. Solar Terr. Phys. 71 (17–18), 1982–1991.
Florescu-Mitchell, A.I., Mitchell, J.B.A., 2006. Dissociative recombination. Phys. Lett. 430 (5–6), 277–374.
Folkestad, K., 1970. Ionospheric studies by *in situ* measurements in sounding rockets, internal NDRE Report 59 (and Ph.D. Thesis University of Oslo).
Friedrich, M., Torkar, K.M., 1988. Empirical transition heights of cluster ions. Adv. Space Res. 8 (4), 235–238.

Friedrich, M., Torkar, K.M., 1995. An attempt to parameterise negative ions in the ionospheric *D*-region. ESA SP-370, 257–261.
Friedrich, M., Harrich, M., Steiner, R.J., Torkar, K.M., Lübken, F.-J., 2004. The quiet auroral ionosphere and its neutral background. Adv. Space Res. 33 (6), 943–948.
Gelinas, Lynette J., Lynch, Kristina A., Kelley, M.C., Collins, S., Baker, S., Friedman, J.S., 1998. First observation of meteoritic charged dust in the tropical mesosphere. Geophys. Res. Lett. 25, 4047–4050.
Havnes, O., Næsheim, L.I., 2007. On the secondary charging effects and structure of mesospheric dust particles impacting on rocket probes. Ann. Geophys. 25, 623–637.
Henry, R.C., Feldmann, P.D., Kruk, J.W., Davidsen, A.F., Durrance, S.T., 1995. Ultraviolet albedo of the moon with the Hopkins ultraviolet telescope. Astron. J 454, L69–L72.
Hervig, M., Thompson, R., McHugh, M., Gordley, L., Russell III, J., Summers, M., 2001. First confirmation that water ice is the primary component of polar mesospheric clouds. Geophys. Res. Lett. 28, 971–974.
Hervig, M.E., Gordley, L.L., Deaver, L.E., Siskind, D.E., Stevens, M.H., Russell, J.M., Bailey, S.M., Megner, Linda, Bardeen, C.G., 2009. First satellite observations of meteoric smoke in the middle atmosphere. Geophys. Res. Lett. 36, L18805. doi:10.1029/2009GL039737.
Jacobsen, T.A., Friedrich, M., 1979. Electron density measurements in the lower *D*-region. J. Atmos. Terr. Phys. 41 (12), 1195–1200.
Jesse, O., 1885. Auffallende erscheinungen am abendhimmel. Met. Zeit. 2, 311–312.
Kieffer, H.H., Stone, T.C., 2005. The spectral irradiance of the moon. Astron. J. 129, 2887–2901.
Leslie, R.J., 1885. Sky glows. Nature 33, 245.
Lübken, F.-J., Rapp, M., 2001. Modelling of particle charging in the polar summer mesosphere: part 2—application to measurements. J. Atmos. Solar Terr. Phys. 63 (8), 771–780.
Lübken, F.-J., von Zahn, U., 1991. Thermal structure of the mesopause region at polar latitudes. J. Geophys. Res. 96 (D11), 20841–20857.
Lynch, Kristina A., Gelinas, Lynette J., Kelley, M.C., Collins, R.L., Widholm, M., Rau, D., MacDonald, E., Liu, Y., Ulwick, J., Mace, P., 2005. Multiple sounding rocket observations of charged dust in the polar winter mesosphere. J. Geophys. Res. 110, A03302. doi:10.1029/2004JA010502.
Mechtly, E.A., Bowhill, S.A., Smith, L.G., Knoebel, H.W., 1967. Lower ionosphere electron concentrations and collision frequency from rocket measurements of Faraday rotation, differential absorption, and probe current. J. Geophys. Res. 72, 5239–5245.
Megner, Linda, Siskind, D.E., Rapp, M., Gumbel, J., 2008. Global and temporal distribution of meteoric smoke: a two-dimensional simulation study. J. Geophys. Res. 113, D03202. doi:10.1029/2007JD009054.
Peterson, J.R., Abert, W.H., Moseley, J.T., Sheridan, J.H., 1971. Ion–ion mutual neutralization cross section measured by superimposed beam technique. III $O_2^+ + O_2^-$, $O_2^+ + NO_2^-$, and $NO^+ + NO_2^-$. Phys. Rev. 3A, 1651–1657.
Phelps, A.V., 1969. Laboratory studies of electron attachment and detachment processes of aeronomic interest. Can. J. Chem. 47, 1783–1793.
Rapp, M., 2000. Capture rates of electrons and positive ions by mesospheric aerosol particles. J. Aerosol Sci. 31, 1367–1369.
Rapp, M., 2009. Charging of mesospheric aerosol particles: the role of photodetachment and photoionization from meteoric smoke and ice particles. Ann. Geophys. 27 (6), 2417–2422.
Rapp, M., Strelnikova, Irina, Strelnikov, B., Hoffmann, P., Hoppe, U.-P., Friedrich, M., Robertson, S., Knappmiller, S., Wolf, Mareille, Marsh, D., 2010. Rocket-borne *in-situ* measurements of meteoric smoke: charging properties and implications for seasonal variations. J. Geophys. Res. 115, DOOI16. doi:10.1029/2009JDO12725.
Roddy, P.A., Earle, G.D., Carlson, C.G., Bullet, T.W., 2004. Relative concentration of molecular and metallic ions in midlatitude intermediate and sporadic *E* layers. Geophys. Res. Lett. 31, L19807. doi:10.1029/2004GL020604.
Sagalyn, Rita C., Smiddy, M., Wisnia, J., 1963. Measurement and interpretation of ion density distribution in the daytime *F* region. J. Geophys. Res. 68, 199–211.
Saunders, R.W., Plane, J.M.C., 2006. A laboratory study of meteor smoke analogues: composition, optical properties and growth kinetics. J. Atmos. Solar Terr. Phys. 68 (18), 2182–2202.
Smith, L.G., 1969. Langmuir probes in the ionosphere, Small Rocket Techniques. North Holland, pp. 1–15.
Smith, I.W.M., 1980. Kinetics and Dynamics of Elementary Gas Reactions. Butterworths, London.
Smith, G.P., Lee, L.C., Cosby, P.C., 1979. Photodissociation and photodetachment of molecular negative ions. VIII—nitrogen oxides and hydrates. J. Chem. Phys. 71, 4464–4470.
Stauning, P., 1996. High-latitude *D*- and *E*-region investigations using imaging riometer observations. J. Atmos. Terr. Phys. 58 (6), 765–783.
Strelnikova, Irina, Rapp, M., Shika Raizada, Sulzer, M., 2007. Meteor smoke particle properties derived from arecibo incoherent scatter radar observations. Geophys. Res. Lett. 34, L15815. doi:10.1029/2007GL030635.
Strelnikova, Irina, Rapp, M., Strelnikov, B., Baumgarten, G., Brattli, A., Svenes, K., Hoppe, U.-P., Friedrich, M., Gumbel, J., Williams, B.P., 2009. Measurements of meteor smoke particles during the ECOMA-2006 campaign: 2. results. J. Atmos. Solar Terr. Phys. 71 (3–4), 486–496.
Strobel, D.F., Young, T.R., Meier, R.R., Coffey, T.P., Ali, A.W., 1974. The nighttime ionosphere: *E* region and lower *F* region. J. Geophys. Res. 79 (22), 3171–3178.
Strobel, D.F., Opal, C.B., Meier, R.R., 1980. photoionization rates in the nighttime *E*- and *F*-region ionosphere. Planet. Space Sci. 28, 1027–1030.
Szuszczewicz, E.P., 1972. Area influences and floating potentials in langmuir probe measurements. J. Appl. Phys. 43 (3), 874–880.
Thrane, E.V., 1974km. ionospheric profiles up to 160 km: a review of techniques and profiles, Methods of Measurements and Results of Lower Ionosphere Structure. Akademie Verlag, Berlin.
Thrane, E.V., Grandal, B., Hagen, O., Ugletveit, F., Bangert, W., Friedrich, M., Loidl, A., Schwentek, H., Torkar, K.M., 1979. Ion production and effective loss rate in the mesosphere and lower thermosphere during the western european winter anomaly campaign 1975/76. J. Atmos. Terr. Phys. 41, 1097–1103.
Thomas, G.E., McKay, C.P., 1985. On the mean particle size and water content of polar mesospheric clouds. Planet. Space Sci. 33, 1209–1224.
Troe, J., Miller, T.M., Viggiano, A.A., 2007. Low-energy electron attachment to SF6. I. Kinetic modelling of nondissociative attachment. J. Chem. Phys. 127, 224303.
Turco, R.C., Sechrist Jr, C.F., 1972. An Investigation of the Ionospheric *D* region at sunrise, 2, estimation of some photodetachment rates. Radio Sci. 7, 717–723.
Woodcock, K.R., Vondrak, T., Meech, S.R., Plane, J.M., 2006. a kinetic study of the reactions $FeO^+ + O$, $Fe^+.N_2 + O$, $Fe^+.O_2 + O$ and $FeO^+ + CO$: implications for sporadic *E* layers in the upper atmosphere. Phys. Chem. 8 (15), 1812–1821.